Matter

CellPress

Perspective

Decisive Structural and Functional Characterization of Halide Perovskites with Synchrotron

Yuanyuan Zhou,[1,*] Hua Zhou,[2,*] Junjing Deng,[2] Wonsuk Cha,[2] and Zhonghou Cai[2]

Halide perovskites have emerged as a new class of inorganic-based soft semiconductors that are revolutionizing the field of (opto)electronics. However, the fundamental structures and properties or functions of halide perovskites are still far from being fully understood, calling for the need of precise, quantitative, and high-spatiotemporal-resolution characterizations. As one of the most powerful multimodal characterization techniques, synchrotron radiation offers high-brilliance X-ray beams for high-resolution observations across multiple length scales obtained within extremely short time spans. Performing a brief review of synchrotron-based perovskite studies in the literature, here we provide perspectives on the use of synchrotron characterizations not only for studying multiple-length-scale structures and dynamic variations of perovskite materials, but also for *in situ* monitoring of device functions and dynamics. The goal of this perspective is to present many capabilities and evoke emerging opportunities of synchrotron characterizations for providing decisive answers to the outstanding science problems in the perovskite field, pushing forward the technological development.

INTRODUCTION

In recent years there has been tremendous interest in halide perovskites (HPs), which are emerging as a new family of functional materials.[1,2] HPs are highly tunable in properties (e.g., optoelectronic, light-emissive, ferroelectric, ionic, magnetic), and are extremely easily solution-processed in various materials forms including thin films, nanocrystals, and single crystals.[3,4] These open up possibilities in their applications to a wide range of devices such as photovoltaics (PVs), light-emitting devices, radiation detectors, ferroelectrics, iontronics, transistors, and spintronics.[4,5] Specifically, perovskite PVs have recently demonstrated a record certified power conversion efficiency of 25.2%, rivaling that of crystalline silicon PVs.[6] There are also recent studies exploring HPs as a new quantum-materials platform, and developing their frontier applications to the future systems of quantum computing, sensing, and information.[7,8] All such technological interests have driven the scientific interest in understanding the fundamental structures of HPs and their correlations to physicochemical properties and device performance.

The most standard HPs have a three-dimensional (3D) crystal structure with a chemical formula of ABX_3, where A is a monovalent organic cation (e.g., $CH_3NH_3^+$, $HC(CH_2)_2^+$, Cs^+), B is a divalent metal cation (e.g., Pb^{2+}, Sn^{2+}, Ge^{2+}), and X is a halide anion (e.g., I^-, Br^-, Cl^-).[4] As illustrated in Figure 1, the HP family has later embraced many new perovskite "members" with reduced crystallographic dimensionalities, such as so-called 2D Ruddlesden-Popper (RP, A_2BX_4) phase, 2D Dion-Jacobson

Progress and Potential

High-spatiotemporal-resolution synchrotron characterization is of great use for gaining insights into structure, property, and device-function landscapes of electronic materials. While the unique advantages of synchrotron X-ray characterization have already been well demonstrated in fields such as batteries and electrocatalysis, its extended application to halide perovskite optoelectronics has just emerged as a new research direction. This perspective discussion ushers a new, rational methodology toward decisive understanding of halide perovskites by synchrotron. The future effort along the perspective research directions may guide the design of more efficient, stable, nontoxic photovoltaics and (opto) electronics, generating profound impacts on renewable energy. Importantly, this discussion also stimulates the development and expansion of synchrotron-based instrumentation and techniques for tailored characterization of many other emerging classes of inorganic-based soft semiconductors beyond halide perovskites.

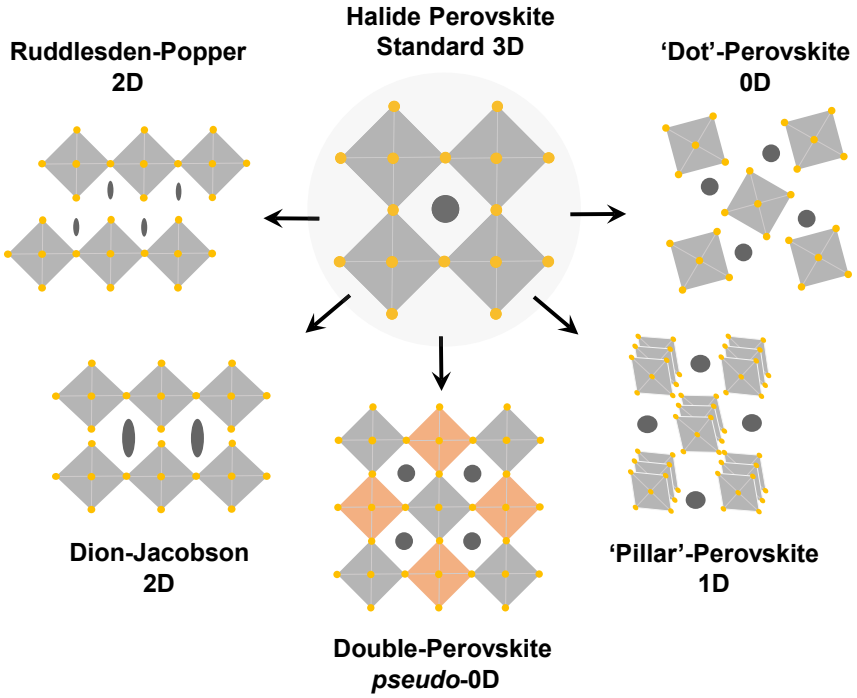

Figure 1. Halide Perovskite Family Tree

Schematic illustration of the broad halide perovskite (HP) family with crystal structures varying from the standard 3D version (original members) to Ruddlesden-Popper 2D, Dion-Jacobson 2D, and double-perovskite pseudo-0D versions (extended members), to "pillar"-HP 1D and "dot"-HP 0D compounds (pseudo-members). Some special types of HP members, such as layered HPs with 2D crystal structure and alternative-cation interlayers, are not included in this schematic.

(DJ, ABX_4) phase, and double perovskites ($A_2B'B''X_6$ or A_2BX_6).[9,10] There are also numerous perovskite-inspired halide compounds, popularly known as "1D perovskites" and "0D perovskites", which consist of "pillar"-like [BX_6] octahedra-connected chains and isolated "dot"-like [BX_6] octahedra, respectively.[11] Due to the structural similarity to perovskites, these compounds have been widely discussed as "pseudo-members" of the broad HP family. Besides, HPs can exhibit very different physical properties and chemical stability when they are formed with mixed phases of different compositions. All such flexibilities in compositions and crystal structures have eventually rendered HPs into an unprecedented material family with an almost unlimited number of derivative-, extended-, or pseudo-members. Regarding the microstructure, HPs exhibit an apparent microstructure similar to those conventional crystalline inorganic semiconductors such as CdTe.[12] In typical HP thin films, the features of grain and grain boundaries are easily observed directly using conventional characterization techniques such as scanning electron microscopy (SEM) with no necessity of additional chemical etching. Moreover, they are highly tailorable by soft chemical methods (e.g., low-temperature solvent/vapor treatment), leading to the emergence of many new and diverse types of thin-film structures.[3]

There have been numerous studies proposing to achieve high-performance functional perovskite devices with various new HP compositions and microstructures, which are highly promising in terms of pushing forward the technological progress.[3,13] Nevertheless, at the same time there are still many inconsistencies in the literature regarding HP-related observations, which are obscuring the "true"

[1]School of Engineering, Brown University, Providence, RI 02912, USA

[2]X-Ray Science Division, Advanced Photon Source, Argonne National Laboratory, Lemont, IL 60439, USA

*Correspondence: yuanyuan_zhou@brown.edu (Y.Z.), hzhou@aps.anl.gov (H.Z.)

https://doi.org/10.1016/j.matt.2019.12.027

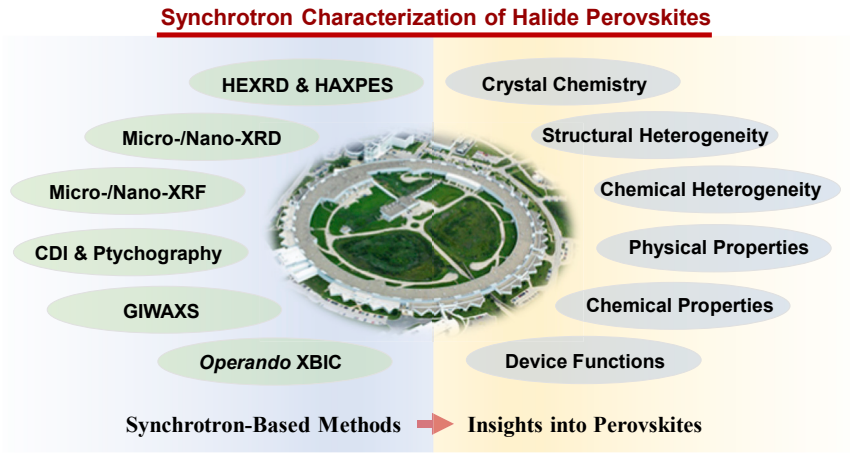

Figure 2. Synchrotron Characterization of Halide Perovskite

Schematic illustration of the technical capability and scientific applications of various synchrotron-based characterization techniques for gaining insights into the science problems in the field of HPs. In the center of this schematic is a photograph of the synchrotron facility at the Advanced Photon Sources at Argonne National Laboratory. Courtesy of Argonne National Laboratory.

composition-microstructure-property-performance relationships and the effective strategies in boosting the HP devices to approach the fundamental limit. This outstanding issue is mostly attributed to the lack of a decisive, nondestructive characterization method for probing the structure and dynamics of HP materials and devices at the small scales. To address this, here we present a perspective discussion on the development of synchrotron-based characterizations for HPs. We introduce the unique capabilities of conventional and advanced synchrotron-based characterization techniques, and briefly review the related efforts reported to date in the literature. In light of scientific and technical motivations, we demonstrate the synchrotron-based characterization of HPs as a new research avenue with vast opportunities for new discovery and advances.

SYNOPSIS OF SYNCHROTRON X-RAY TECHNIQUES: EXISTING AND EMERGING

Since the early development of storage-ring-accelerator-based synchrotrons declared its independence out of parasitic phase with high-energy physics facilities, the gigantic X-ray source has evolved into one of the mainstream scientific tools essential in tackling challenging scientific problems, in particular leading to transformational levels of insights for our ability to explore, understand, and create a variety of new materials that would bring about enormous technological and societal impacts in engineered structures, modern electronics, sustained energy sources, and a host of other applications. The advances in materials discoveries enabled by versatile X-ray techniques derived from the three major pillar categories of scattering, spectroscopy, and microscopy have been tremendous and long-lasting, concertedly propagated both by emergence of new fundamental ways to understand the interaction of X-rays with a variety of materials and by the evolution of light sources themselves.

In respect of material characterizations of the booming HP family and extended members, matured and ever-improved synchrotron X-ray techniques for quantifying crystal structures, chemical compositions, and electronic energy landscapes had been readily utilized since the early stage of HP discovery and development, as illustrated in Figure 2. The comprehensive review of existing works routinely using X-ray

diffraction (XRD) and spectroscopy is too extensive to remain within the scope of our perspective. In this section, therefore, we merely provide a few selective outstanding cases on the determination of much more complex crystal structures and symmetries of derivative HP families such as layered 2D systems. The *in situ* X-ray technique, grazing incidence wide-angle X-ray scattering (GIWAXS), albeit adopted in most studies of HP thin films and multilayered solar cell devices, is still deserving of attention owing to the merit that it permits fast capture of transient processes and metastable intermediate phases on crystallization, transformation, and degradation of HPs. Other than deep X-ray penetration power and wide X-ray energy tunability, the lasting improved brightness of the state-of-the-art synchrotron source could convert many conventional scattering and spectroscopy techniques into microscopic and imaging modalities to render multidimensional mapping of studied materials and devices with sufficiently high spatiotemporal resolution to capture events of interest.[14] One main theme of our perspective is to introduce the frontier of X-ray microscopy/imaging techniques nevertheless much practiced by the HP field, and to elaborate the emerging and tentative examples utilizing various mission-specific X-ray microscopies, in particular the use of advanced micro-/nanoscale imaging, such as micro-/nano-XRD and X-ray fluorescence (micro-/nano-XRF), and coherent X-ray scattering techniques, such as Bragg coherent diffractive imaging (BCDI)[15] and ptychography,[16] in revealing detailed microstructures, subtle lattice strain profile, and local elemental fluctuations. Moreover, one pressing direction within the scope of X-ray microscopy to highlight in the last part of this perspective is the unique *in operando* correlative microscopy by tracking X-ray beam induced current (XBIC) (see, e.g., in-depth description in Stuckelberger et al.[14]), which directly links microstructure/composition information to local optoelectronic responses of an HP device at the meso-/nanoscale.[14]

As the flip side of the coin, remarkable flexibilities in compositions and structural building blocks of many HP systems also make the materials very susceptible and sensitive to external stimuli and disturbance even in the very cautious process of material characterizations, which largely dethrone most destructive and post-processed probes, including commonly used electron microscopy, due to degrading effects induced by severe electron beam irradiation.[17] Although X-ray techniques bear significant advantages on nondestructive material characterizations of HP materials owing to much weaker X-ray matter interactions, high X-ray dose or dose density from a high-brightness, high-flux synchrotron source may nonetheless give rise to very pronounced sample damage or irreversible transformations beyond intrinsic aging mechanisms, especially the highly focused beam in use. More careful and precise sample environment controls (e.g., oxygen, moisture, heat, and light) in concert with intelligent X-ray dose management need to be implemented and optimized to mitigate the undesirable X-ray beam effects. For instance, in scanning X-ray microscopy, advanced motion control and flying-mode beam trajectory have been demonstrated to effectively minimize local beam exposure while preserving highly efficient image acquisitions.[18]

FRONTIERS IN SYNCHROTRON-BASED STUDIES OF HALIDE PEROVSKITES

In the literature there have been tantalizing synchrotron-based studies on HPs, which have led to important findings that are related to their key aspects, including refined (super)lattice symmetry,[19,20] dynamic disorder,[21,22] grain-boundary phenomenon,[23] nanoscale chemical/phase heterogeneity,[24] pressure-/temperature-dependent phase transition,[25–27] strain effects,[28,29] solution-based crystal growth

modes,[30–32] degradation mechanisms,[33] and nanoscale device responses.[24,34,35] In the following sections, we discuss these established research works as well as some preliminary results that demonstrate the capability of synchrotron-based characterization in advancing our fundamental understanding of HP materials and devices.

Determination of Crystal Structures, Compositions, Band Profiles, and Textures

The materials properties and device performance of HPs are highly dependent on their intrinsic crystal structures, compositions, and band-gap profiles. Thus, various crystal, composition, and band-gap engineering strategies have been proposed for improved device efficiency and stability, which include (1) crystal-dimensionality tailoring via large organic-molecular cation incorporation, (2) ionic doping/alloying at either A, B, or X site, and (3) crystallographic texture development. Determination of such resulting new perovskite structures calls for the use of synchrotron-based hard or high-energy XRD (HEXRD), GIWAXS, and X-ray absorption spectroscopy (XAS), as well as hard X-ray photoemission spectroscopy (HAXPES).

The standard 3D HPs such as $MAPbI_3$ and $FAPbI_3$ exhibit simple crystal structures and are relatively easy to characterize using laboratory X-ray diffractometers. However, the layered 2D HPs, which have attracted increasing attention in the perovskite field, possess much more complex crystal structures and symmetries. Layered 2D HPs can be formed different layer numbers (n) of corner-, edge-, or face-shared octahedra with large organic-molecular cation (either monovalent or divalent) interlayers, which creates superstructures at the molecular level. XRD characterization and determination of such complex hierarchical crystal structures is obviously challenging. Especially for these high-member layered 2D HPs ($n > 5$), the interplane distances of the characteristic ($0k0$) basal planes could be as large as a few tens of angstroms. Because of the high interference from thick crystalline octahedra slabs between the basal planes, the characteristic ($0k0$) reflections obtained by laboratory X-ray diffractometers can be extremely weak, for which high-energy synchrotron-based XRD (SXRD) will be needed. Kanatzidis and coworkers[20] recently reported a successful synthesis of high-member Ruddlesden-Popper 2D perovskite phases of $BA_2MA_{n-1}Pb_nI_{3n+1}$ with $n = 6$ and $n = 7$. The crystal structures of these two phases are schematically shown in Figure 3A. SXRD patterns of $BA_2MA_{n-1}Pb_nI_{3n+1}$ ($n = 3$ to 7, and $n = \infty$) are compared in Figure 3B. The indexed (020) and (040) reflections are characteristic basal planes for the 2D layered superstructures. It can be seen that the intensities of these two reflections significantly decrease with an increase of n. Nevertheless, owing to the high energy of synchrotron irradiation, these two characteristic reflections in $BA_2MA_{n-1}Pb_nI_{3n+1}$ with $n = 6$ and $n = 7$ are still observed, providing unambiguous evidence for the existence of these high-member Ruddlesden-Popper layered 2D perovskites. This discovery expands the understanding of the thermodynamic limit of n in 2D perovskites, which is key to revealing the mechanisms of 2D perovskite-based devices.

Crystallographic orientation or texture is another important structural characteristic of semiconductor crystals, as a texture development may provide unique electronic properties. For HPs, it is further closely related to the chemical stability. The texture of HP crystals can be directly visualized, even quantitatively, using GIWAXS. Very recently, Steele et al.[36] used GIWAXS to study the structure of $CsPbI_3$ (in thin-film form on a rigid glass substrate), which is kinetically stabilized as perovskite phase from a thermal-quenching process. In Figure 3C, anisotropic in-plane ($q_{x,y}$) and out-of-plane (q_z) peak splittings are observed, which is a clear signature of crystallographic texture. Such a texture development has been attributed to the

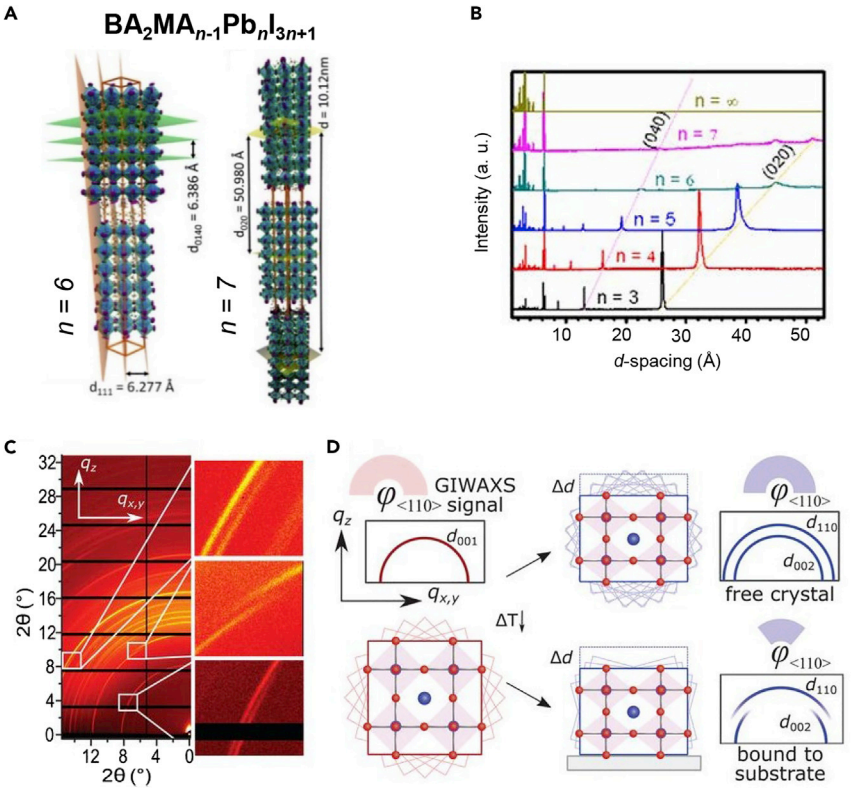

Figure 3. Crystal Structure Determination of Halide Perovskites

(A) Schematic illustration showing the crystal structures of 2D Ruddlesden-Popper HP $BA_2MA_{n-1}Pb_nI_{3n+1}$ phases with $n = 6$ and $n = 7$.

(B) Synchrotron-based XRD (SXRD) patterns for $BA_2MA_{n-1}PbI_{3n+1}$ perovskite phases with different n ($n = 3$ to 7, and $n = \infty$). Data were collected at the beamline 11-BM-B of the Advanced Photon Source, Argonne National Laboratory. Adopted from Soe et al.[20] under either a CC BY-NC-ND or CC BY license.

(C) GIWAXS pattern of a $CsPbI_3$ perovskite thin film prepared by a thermal-quenching process from high temperature (330°C) to room temperature.

(D) Schematic illustration of diffraction ring splitting in the GIWAXS signal when the $CsPbI_3$ crystal forms a heterojunction with the substrate at high temperature and undergoes tensile strain and texture formation (with angular distribution ϕ) upon quenching. Data were collected at the BM01 of SNBL/ESRF (European Synchrotron Radiation Facility) in Grenoble, France and at the NCD-SWEET beamline of ALBA in Cerdanyola del Vallès, Spain. Adopted from Steele et al.[36] with permission requested from American Association for the Advancement of Science.

perovskite-substrate interface that "pins" the initial anisotropic cubic $CsPbI_3$ unit cell, as illustrated in Figure 3D.

Ionic doping and alloying in HPs are enabled via extremely facile ion exchange or displacement reactions, which have contributed to the performance in the state-of-the-art perovskite devices such as so-called triple-cation perovskite PVs.[37] However, the doping or alloying mechanisms are usually obscured, which can be more clearly revealed with the aid of a synchrotron. Chen et al.[38] have studied Ag-doped HP thin film using synchrotron-based extended X-ray absorption fine structure (EXAFS) spectra (obtained at Line BL14W1 of the Shanghai Synchrotron Radiation Facility). The analysis of the Ag *K*-edge EXAFS spectrum shows that the coordination number (5.9) of Ag is close to that (4.0) of Pb, concluding that Ag is primarily doped at B sites in HPs. In most cases XAS probes the variation of chemical composition,

local bonding, and coordination information through the bulk of a sample (e.g., deep penetration depth) unless the total-electron-yield mode is adopted usually in soft X-ray regime (typically less than 2–3 keV) or the grazing incidence geometry is utilized typically for the case of thin films with good flatness. In contrast, XPS probes mostly the very top surface chemical and electronic information due to the very shallow escape depth (typically a few angstroms or a few monolayers) of low-energy X-ray induced photoelectrons if a regular soft X-ray source is used (either lab source or synchrotron). Nevertheless, the wide energy tunability of the synchrotron source endows the unique depth-profile technique of HAXPES, which can render a continuously varied probing depth by changing the X-ray photon energy via a high-resolution X-ray monochromator. In last few years, HAXPES has been actively utilized in studies detecting doped or incorporated cations and determining the chemical distribution and electronic configurations of HP films profiled from surface to bulk.[39,40] Philippe et al.[39] delivered the cation depth profiling of HP materials containing multiple monovalent cations (e.g., Cs^+, Rb^+, MA^+, FA^+) by HAXPES. Abdi-Jalebi et al.[40] investigated the HP structures incorporating Na^+, Cu^+, and Ag^+ by HAXPES, which showed a large shift in the valence band position for Cu- and Ag-doped films toward the middle of the unaffected band gap. The distinct valence band shift gave the clue that incorporation of these monovalent cations anti-doped the intrinsic *n*-type HP films without these added cations. In addition to chemical distributions, core-level and valence-level XAS (e.g., probing both unoccupied and occupied states) and XPS (e.g., bulk-sensitive HAXPES) are also suitable for mapping out the semiconducting band profiles and the relevant electron states in the vicinity of the Fermi level.

Multidimensional Mapping of Halide Perovskite Structures at the Nanometer Scale

Thin films are the primary form of HP materials in the device setting. Most HP thin films studied are polycrystalline.[3,12] The characteristics of grain boundaries and grains, as well as distributions of chemical compositions and phases within thin films, can have very significant impacts on the physical processes (e.g., carrier transport, emission), chemical properties (e.g., ionic/molecular diffusion, environmental stability), and optoelectronic device performance. The soft nature of HP thin films makes it challenging to characterize their microstructural/compositional features using conventional high-resolution techniques such as transmission electron microscopy (sample preparation usually requiring focused ion beam [FIB]), as high-energy electron or ion beams easily induce the transformation of their original microstructural and compositional features.[41] SEM-based and atomic force microscopy (AFM)-based characterizations have been widely used in the perovskite field for identifying grains and grain boundaries based on the morphology and topography, which only provide limited and sometimes misleading results. For example, Li et al.[42] demonstrated that there are in fact invisible grain boundaries existing in apparent single grains (under SEM and AFM) based on photoluminescence microscopy, but the character of such grain boundaries still remains unknown. At the other extreme, the apparent grain boundaries (under SEM and AFM) are sometimes just physical boundaries of macroscale grain clusters, instead of the true grain boundaries.[3] In this regard, synchrotron-based X-ray microscopy, in particular coherence-based X-ray imaging, provides a deterministic characterization of micro-/nanostructures with tolerable and mitigated radiation damage to samples. Tentative efforts have been made in using synchrotron-based X-ray microscope imaging to reveal the crystallographic structures of grain boundaries, to study local strains, and to obtain correlated microstructure-composition tomography in HP thin films, which are leading toward significantly advanced understanding of HP thin-film microstructures.

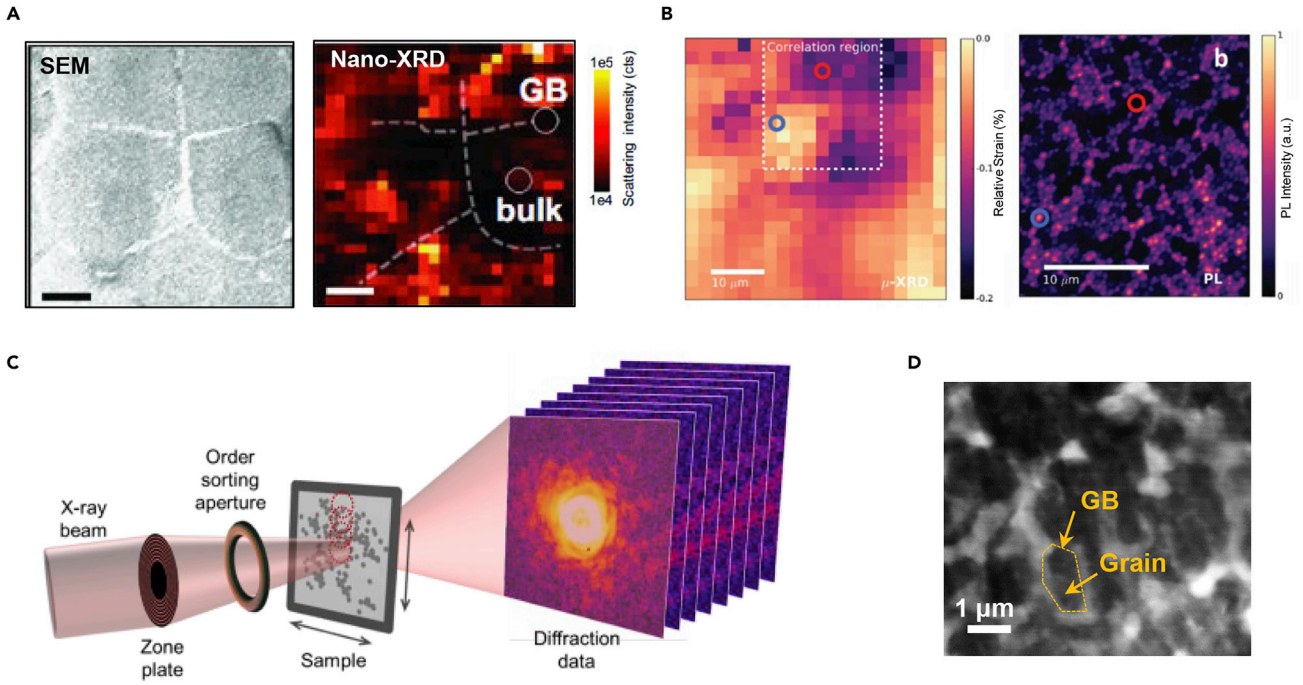

Figure 4. Multidimensional Imaging of Halide Perovskite

(A) SEM image (left panel) and correlated synchrotron micro-/nano-XRD map (right panel) of the grain-boundary region in a $MAPbBr_3$ perovskite thin film. In the micro-/nano-XRD map, the brightness indicates summed scattering intensity across the (002) peak of $MAPbBr_3$ by rocking θ. Scale bars represent 4 μm. Micro-/nano-XRD data were collected at sector 26-ID-C of the Advanced Photon Source, Argonne National Laboratory. Adopted from Adhyaksa et al.[23] with permission requested from Wiley.

(B) Strain map (left panel) of an $MAPbI_3$ perovskite thin film based on the relative shift of the peak q value at each local point from the minimum q in a micro-XRD map. Note that $q = 4\pi \sin(\theta)/\lambda$, where θ is the angle between incident beam and the crystallographic reflecting plane and λ is the X-ray incidence wavelength. Here strain is estimated by $(q_{min} - q)/q_{min}$. Right panel: confocal PL map (405 nm laser excitation) of the dashed region in the strain map. The micro-/nano-XRD data were collected at the ID13 beamline at the ESRF with beam spot size 200 × 200 nm^2. Adopted from Jones et al.[28] under a Creative Commons Attribution 3.0 Unported Licence.

(C) Schematic of X-ray ptychography measurement reconstructing buried nanostructures of samples located on an X-ray-transparent silicon-nitride window. Courtesy of Dr. Johanna Nelson Weker and Dr. Anna M. Wise at SLAC National Accelerator Laboratory.

(D) A typical 2D reconstructed X-ray ptychographic image of an HP sample (inorganic $CsPb_{0.6}Sn_{0.4}I_3$ perovskite crystalline thin films with grain boundaries coated by low-contrast SnF_2 phase; preliminary results collected at the Velociprobe at the Advanced Photon Source, Argonne National Laboratory).

Grain boundaries play a key role on the performance of inorganic-based thin-film optoelectronic devices, but their effects in HP materials and devices are yet to be elucidated. The characteristics of HP grain boundaries such as misorientation, degree of disorder, local chemistry, and secondary phase have been less correlated with the properties and device performance. Adhyaksa et al.[23] demonstrated the use of synchrotron micro-/nano-XRD for probing grain boundaries in a polycrystalline $MAPbBr_3$ HP thin-film sample. This sample shows an apparent grain size of a few tens of micrometers from the SEM image shown in the left panel of Figure 4A. The summarized scattering intensities of the characteristic (002) peak of $MAPbBr_3$ by rocking θ are mapped across the same sample region in the SEM image. The resulting micro-/nano-XRD map (right panel of Figure 4A) shows no obvious scattering at the grain-boundary regions, implying that grain boundaries in large-grain $MAPbBr_3$ HP thin films are amorphous. While this study presents an interesting example in probing HP grain boundaries using a synchrotron, there are rich possibilities in discovering a lot more new grain-boundary phenomena in HPs by extending research in this direction. One of the most essential grain-boundary phenomena is coherent twinning that is frequently observed in PV semiconductor materials and

also recently observed in HP thin films.[22,43] Using synchrotron-based techniques to establish a clear relationship between the microstructure of coherent twinning and the optoelectronic properties in HPs might reveal the hidden mechanisms of high-performance perovskite PVs.

The residue strain in the HP thin films has recently drawn a lot of attention in the perovskite field.[32] Zhao et al.[44] are the first to demonstrate the presence of residue strain in typical solution-processed HPs based on laboratory XRD, which is produced due to the thermal expansion coefficient mismatch and cubic-to-tetragonal phase transition during the solution processing. It has been later shown that such residue strain strongly influences the recombination processes and chemical stability in HPs. To reveal the local residue stain at the nanoscale in HP thin films and its correlation with carrier recombination, Jones et al.[28] performed a study by combining synchrotron micro-/nano-XRD and confocal time-resolved photoluminescence (PL) microscopy. Figure 4B shows a map of nanoscale residual strain and a correlated map of PL lifetime. It reveals that the residue strain in the $MAPbI_3$ HP thin film has a complex heterogeneity and is directly associated with enhanced nonradioactive recombination. In another study by Li et al.,[29] the effect of nanoscale residual strain on HP structural stability was also studied using synchrotron micro-/nano-XRD. It was found that in a solution-synthesized $CsPbBr_3$ HP thin film, a strain gradient develops within in the HP crystal, which was revealed by a 2D nano-XRD map (not shown here). The regions with reduced strains were found to exhibit better chemical stability, which suggests a new way to mitigate the HP instability issue through reducing local strains.

For identifying grain distributions and grain boundaries across the mesoscale field of view, coherent X-ray based ptychography combining the power of scanning X-ray microscopy with BCDI, can be utilized for the multidimensional rendering of internal states (e.g., microstructure and morphology) of complex materials by using both quantitative absorption and phase contrast for visualization. Figure 4C schematically illustrates the experimental layout and scanning trajectory of X-ray ptychography adopting the transmission geometry. A series of coherent diffraction patterns are collected as the coherent and focused X-ray beam is scanned across the sample. Correlated iterative phase retrieval analysis among neighboring scanned spots can reconstruct the overall electron density profile/volume across the sample with a spatial resolution better than the focused spot size and fundamentally limited by X-ray wavelength and accumulated dose on the sample. In comparison, the spatial resolution of regular scanning micro-/nano-XRD or XRF is usually limited by the focused spot size that is determined by X-ray focusing optics. Figure 4D demonstrates a preliminary imaging result of a reconstructed 2D ptychogram of a $CsPb_{0.6}Sn_{0.4}I_3$ perovskite polycrystalline thin film, where the grain interior and grain boundary with obviously distinct contrasts are distinguished. By rotating the sample, a tomographic-like series of 2D ptychograms can eventually lead to a full 3D density distribution of the polycrystalline perovskite sample. Such a quantitative 3D nanoimaging method has been used to study organic tandem solar cells based on water-processed nanoparticles.[45] As a scanning imaging technique, X-ray ptychography can be naturally combined with other scanning microcopy techniques, such as XBIC and XRF, to study perovskite materials in one experiment. Such a correlative imaging[46] with different contrast modalities (e.g., nanostructure, chemical composition, local optoelectronic property) would deepen our understanding of the sample while reducing the total radiation dose accumulated on the sample compared with the sequential imaging approach and alleviate damage from exposing the sample to different imaging conditions. X-ray ptychography can also be combined with XAS to

map the chemical composition of perovskite materials with high spatiospectral resolution by conducting an X-ray ptychography series across the absorption edges of target elements.[47,48] In addition, if one collects the coherent XRD patterns near a certain Bragg condition (e.g., vicinity of a particular *hkl* Bragg peak) exiting from an isolated crystalline object, the lattice displacement distribution within the individual crystal can be further extracted in addition to 3D morphology of the sample by retrieving the phase of the diffracted waves. Recently, this unique capability of BCDI has enabled imaging of individual grains in polycrystalline thin films and reveals strain distribution as well as dynamics of dislocations.[49]

In Situ Characterization of Materials Dynamics (Crystallization, Degradation, Transformation)

In situ synchrotron-based studies on crystallization, transformation, and degradation of HPs can capture the metastable intermediate phase, which can further be correlated with the morphology/microstructure changes at multiple-length scales. This is key to searching for novel methods that can better tailor these dynamic processes for high-performance perovskite devices.

HPs are crystallized from precursor solutions either directly, based on the "self-assembly" of solution ions (the so-called one-step method) or sequentially, based on the reaction of one predeposited precursor phase with the other (the so-called two-step method).[3,12] For the former, HPs nucleate directly from the solution, followed by grain growth. In the presence of strong coordination of the solvent or additive molecules with the as-formed perovskite in solutions, the first nucleated phase is a perovskite-solvent complex instead of perovskite itself.[3,12] Additives may also mediate such crystallization by forming new intermediate phases.[3,12] In revealing the particular crystallization mechanisms, GIWAXS has become a very useful tool for tracking phase evolution and transformation during the HP crystallization that occurs in a rapid manner.[50,51] Figure 5A schematically illustrates a typical experimental setup for *in situ* crystallization studies of solution-processed semiconductors, which has been widely applied in the field of organic semiconductors. Here, a doctor blading setup and a heating unit are integrated for coating the solution film and inducing the crystallization in controlled gas environments (e.g., dry N_2 or weakly scattered He), respectively. In a recent study, Hu et al.[30] performed an early synchrotron-based GIWAXS study for understanding the one-step crystallization kinetics of $MAPbI_3$ HP. In their experiment, the precursor solution was a mixture of 0.4 M $PbAc_2$ and 1.2 M MAI in *N*,*N*-dimethylformamide (DMF), and 300 GIWAXS 2D image frames were collected at a speed of 5 s per frame for monitoring the whole crystallization process (starting from the solution state, ending at the solid HP thin-film state). Figure 5B plots *in situ* integral GIWAXS patterns along with time based on all 300 collected frames, and Figure 5C correspondingly plots the variations of peak intensity/position as a function of time. In the low q region, a broad diffuse reflection (Peak A) at $q \sim 0.4$ Å^{-1} is initially observed, which is characteristic of the scattering from the dissolved components. The reflection gradually shifts to higher q as time increases, which implies the formation of aggregates ("building blocks" for crystals). In the high q region, the initial broad diffraction peak ($q \sim 1.5$–2.5 Å^{-1}) is related to the intramolecular packing of solvent molecules, which is reduced along with the rapid evolution of $MAPbI_3$ HP roughly at frame 180 (900 s). Both Peak A and Peak B intensities decrease roughly at frame 180 (~900 s) with the rapid emergence of $MAPbI_3$ HP and perovskite-solvent complex phases. Hu et al.[30] further studied the detailed phase evolution at various temperatures, providing a complete thermodynamics "picture" of the one-step perovskite crystallization. Antisolvent dripping is another popular method for tailoring HP crystallization and making smooth HP

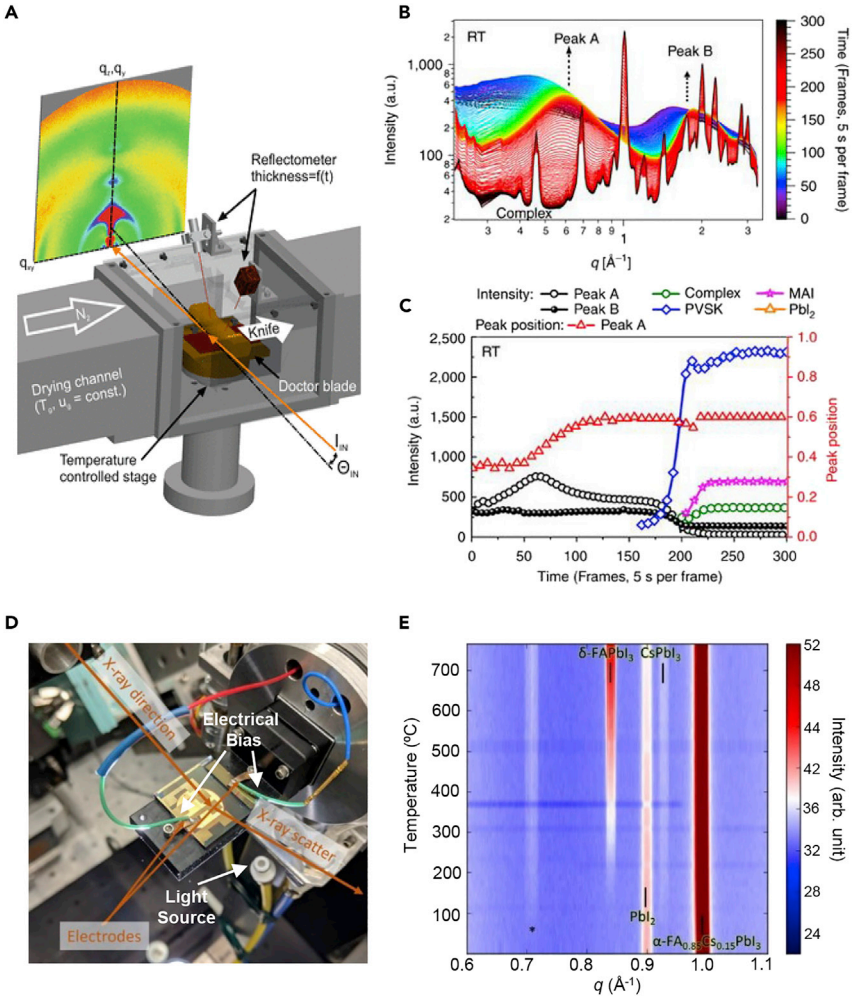

Figure 5. *In Situ* Characterization of Materials Dynamics of Halide Perovskites

(A) Schematic illustration of the experimental setup for *in situ* crystallization studies of HPs and other solution-processed semiconductors using synchrotron-based GIWAXS. The stage is integrated with a doctor-blading setup and heating control.

(B) Corresponding *in situ* integral GIWAXS profiles along with time for the thin films that are crystallized at room temperature (RT) from a perovskite precursor solution. The precursor solution is made with 0.4 M $Pb(Ac)_2$ and 1.2 M MAI in DMF solvent. In total, 300 GIWAXS pattern frames are collected with 5 s per frame for capturing the whole crystallization process.

(C) Corresponding intensity and position variations of characteristic diffraction peaks as a function of heating time. Raw data in (B) and (C) were collected at beamline 7.3.3 at the Advanced Light Source, Lawrence Berkeley National Laboratory.

(D) The custom-built climate chamber used for *in situ* SXRD measurements with the abilities of environmental-condition (light and humidity) control and photocurrent-voltage characterization.

(E) *In situ* SXRD profiles versus device operation time of $FA_{0.85}Cs_{0.15}PbI_3$ perovskite. The peak at ~0.7 $Å^{-1}$ is associated with a hydrate phase (marked by an asterisk). The environmental condition is 50% relative humidity and 1-sun-intensity light. Raw data were collected at the Stanford Synchrotron Radiation Light Source.

(A) is adopted from Schmidt-Hansberg et al.[53] with permission from the American Chemical Society. (B) and (C) are adopted from Hu et al.[30] with permission from Creative Commons. (D) and (E) are adopted from Schelhas et al.[54] with permission from the Royal Society of Chemistry.

thin films. In a more recent study, Bruening and Tassone[31] developed an in-house XRD chamber that enabled the tracking of phase evolution upon antisolvent dripping. Based on various solvent systems forming $MAPbI_3$ HP, it was found that

antisolvent dripping alters the crystallization route by avoiding the formation of metastable intermediate phases, thus leading to fast HP nucleation and smooth HP thin films. Synchrotron GIWAXS has been also applied by Alsari et al.[50] and Stone et al.[51] to study the role of additives on HP crystallization, and by Miyadera et al.[52] to probe the formation kinetics of HPs in the two-step method.

The stability of HP materials and devices is critical for the future deployment of HP technologies in the real world. Understanding the degradation mechanisms of HPs under various environmental conditions (such as temperature, moisture, oxygen, and light) is the prerequisite for finding effective HP stabilization methods. Yang et al.[55] employed synchrotron-based GIWAXS to study *in situ* the $MAPbI_3$ HP degradation in an environmental chamber with controlled relative humidity. By monitoring phase changes in the perovskite degradation process, they identified that the formation of a hydrated intermediate containing isolated $[PbI_6]$ octahedra is the first step of moisture-induced HP degradation. Later, Zhao et al.[33] performed a more systematic synchrotron GIWAXS study coupled with microscopy and gravimetric analyses, further showing that moisture induces phase transformation of $MAPbI_3 \rightarrow MAPbI_3 \cdot xH_2O \rightarrow PbI_2 + MAI$ and then changes the distribution of the decomposition products that causes irreversible $MAPbI_3$ HP hydrolysis. While these early studies have focused on the overall chemical phase transformation during the degradation process, it is envisioned that by combining *in situ* synchrotron-based GIWAXS with the synchrotron-based nanoprobe methods, the effect of micro-/nanostructures, local compositions, and strains on moisture-induced HP degradation will be revealed in great detail. Furthermore, the evaluation of HP stability in an operating perovskite device under a complex environmental condition is practically more useful. In this regard, Schelhas et al.[54] developed a new *in situ* XRD chamber that allows the mounting of a perovskite solar cell and the SXRD measurement at the operation status and controlled environmental conditions (light and humidity). The photograph of this setup is shown in Figure 5D. They studied the phase demixing behavior of α-$FA_{0.85}Cs_{0.15}PbI_3$ HP in perovskite solar cell devices. The *in situ* data in Figure 5E shows that under the stresses of light and humidity for ~90 min, α-$FA_{0.85}Cs_{0.15}PbI_3$ alloy HP partially segregates to its constituent phases (hexagonal δ-$FAPbI_3$ and orthorhombic δ-$CsPbI_3$), which is responsible for the device performance decay (measured *in situ* using the electrical-bias setup attached to the XRD chamber; data not shown). This represents a model study connecting the *in situ* HP degradation studies to solar cell device performance using a tailored synchrotron facility.

In situ probing of HP structural dynamics under extreme stimuli such as high pressure is another interesting direction of fundamental research in the perovskite field. In Figure 6A, an *in situ* high-pressure HEXRD setup using a diamond anvil cell is schematically illustrated. By using this setup, Wang et al.[56] studied the correlated phase transition and optical response of $MAPbBr_3$ HP under hydrostatic pressure up to 34 GPa. The 2D HEXRD patterns of $MAPbBr_3$ HP at various pressures are shown in Figure 6B. As seen, the original $MAPbBr_3$ HP at 0 GPa exhibits strong Debye rings initially. When loading pressure increases, some sharp Debye rings start to weaken while some new broad rings emerge, which indicates the increase of structural disorder and partial amorphization upon pressure. When the loading pressure is larger than 12.5 GPa, all original diffraction rings disappear and only four broad rings remain, indicative of a complete amorphization in $MAPbBr_3$ HP. Wang et al.[54] also found that such pressure-induced $MAPbBr_3$ HP structural dynamics strongly affects the optical responses (e.g., band gaps, photocurrents), shedding light on the exploration of new HP phases for optoelectronic applications. Another promising study by

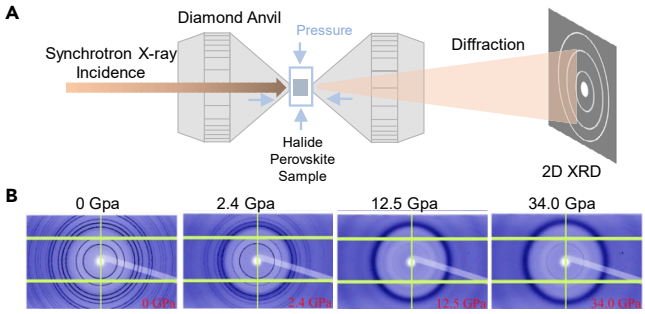

Figure 6. Halide Perovskites Under High-Pressure

(A) Schematic illustration of an *in situ* high-pressure HEXRD setup using a diamond anvil cell.

(B) 2D SXRD patterns of $MAPbBr_3$ under various pressure. Data were collected at 16 ID-B station of High-Pressure Collaborative Access Team at the Advanced Phonon Source, Argonne National Laboratory. Adopted from Wang et al.[56] with permission from the American Chemical Society.

Liu et al.[57] demonstrated that by *in situ* monitoring of structure-property dynamics during the compression and decompression cycle, a new metastable phase of 2D HP $(CH_3(CH_2)_3NH_3)_2MA_{n-1}Pb_{n+1}I_{3n+1}$ (n = 3) was discovered, which exhibits a favorably lower band gap of 1.78 eV than that (1.94 eV) of the conventional phase.

Operando Characterization of Halide Perovskite Optoelectronic Devices

By using a synchrotron irradiation with a highly focused spot size (down to 25 nm) as the device-operation light source, *operando* characterization of perovskite optoelectronic devices can directly correlate the HP microstructure/composition to optoelectronic behavior of perovskite devices at the micro-/nanometer scale. Such *operando* characterization is performed by monitoring XBIC in a working perovskite optoelectronic device (e.g., solar cells, X-ray detectors) in conjunction with synchrotron nano-XRF, as schematically shown in Figure 7A. Stuckelberger et al.[14,34] compared XBIC with the electron-beam-induced current (EBIC) methods, and summarized the following potential advantages of XBIC. First, X-ray has a much higher penetration depth into the device or thin film than electrons, better revealing the bulk information. In addition, XBIC samples are easy to prepare. Unlike EBIC, a FIB lamellae sample is usually required, while FIB easily damages HPs. Furthermore, XBIC experiments can be conducted under various environmental conditions, which is extremely suitable for device degradation studies. Finally, the combination of XBIC and nano-XRF can simultaneously map the elemental composition and charge collection within a selected device region.

The synchrotron-based XBIC-XRF method has exceptional promise for studying perovskite solar cells. In these state-of-the-art perovskite solar cells, the HP layers are mostly made with very complex compositions such as $(MA,FA,Cs,Rb)Pb(I,Br)_3$. In such HP layers, the exact composition at the micro-/nanoscales and its relationship with device performance have been poorly understood. In a recent report, Correa-Baena et al.[24] made tentative efforts to employ XBIC-XRF to study the role of the alkali-metal cations in perovskite solar cells. Figures 7B and 7C are a set of correlated nano-XRF and XBIC profiles of a $(MA,FA)Pb(I,Br)_3$ HP-based solar cells with 5% RbI doping. As seen in the nano-XRF map (Figure 7B), 5% RbI doping induces the formation of Rb-rich clusters within the thin film, and the corresponding XBIC map (Figure 7C) shows obviously reduced photocurrent response at these Rb-rich clusters. These results directly prove that overdoping of RbI forms recombination-active regions in perovskite solar cells and hinders the carrier collection. We envision that future *operando* analyses of various HP devices under various

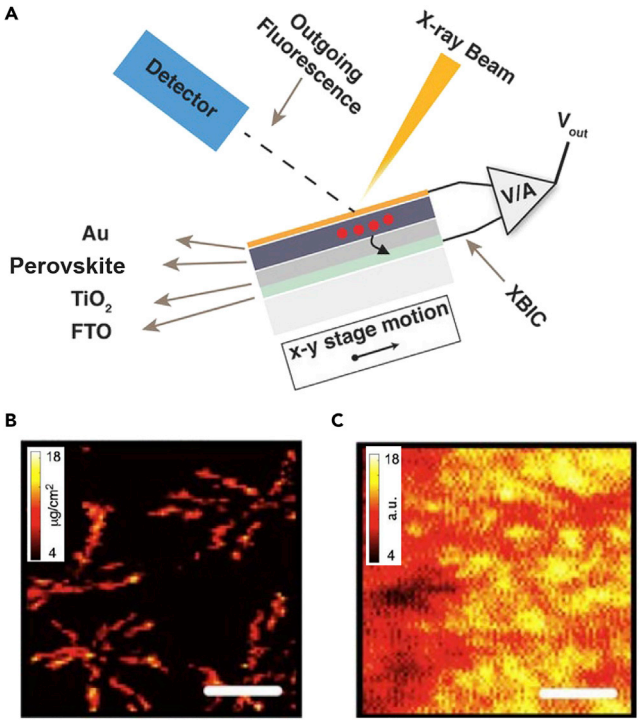

Figure 7. *Operando* Imaging of Halide Perovskite by X-Ray Beam-Induced Current

(A) Schematic illustration of X-ray beam induced current (XBIC) setup for monitoring the nanoscale photovoltaic behavior in a perovskite solar cell. X-ray fluorescence (XRF) measurement is coupled to provide correlated composition-performance results. The stage is movable for obtaining correlated 2D XBIC and XRF maps. Adopted from Luo et al.[35] with permission from Wiley.

(B and C) XRF (B) and XBIC (C) maps of a perovskite solar cell device with an architecture of FTO/TiO_2/HP/Spiro-OMeTAD/Au. The HP layer is made of (MA,FA)Pb(I,Br)$_3$ HP with 5% RbI addition. Scale bar represents 5 μm. Data were collected in a helium environment at beamline 2-ID-D of the Advanced Photon Source, Argonne National Laboratory. Adopted from Correa-Baena et al.[24] with permission from the American Association for the Advancement of Science.

environmental conditions, in conjunction with other *ex situ* synchrotron-based nanoprobes, will provide many valuable insights into the operation and degradation mechanisms.

ADVANCES IN SYNCHROTRON TECHNIQUES AND THEIR IMPACTS ON HALIDE PEROVSKITE RESEARCH

In the next 5–10 years, storage ring-based synchrotron light sources across the globe will take a transformational level of advance: upgrading electron accelerators to adopt the multibend achromat (MBA) lattice design of magnets array, which will boost the resulting X-ray beam brightness and coherence by 2–3 orders of magnitude.[58,59] Ongoing facility upgrades such as the Advanced Photon Source Upgrade (APS-U) represent a landmark in such a trend. The vast technical leaps in X-ray beam properties in pace with rapid advancements in focusing optics, undulators, detectors, computing, and theory will holistically transform all existing X-ray detection modes into very powerful and informative imaging modes to explore all aspects of materials that previously were scarcely accessible.[60]

From this perspective, highly focused X-rays down to submicron-scale and nanoscale, permitting one to acquire more sampling in greater detail and in a shorter

time, will be routinely accessible to interrogate existing and emerging HP materials. Structural, compositional, and electronic inhomogeneity across the HP sample will be efficiently mapped and recorded. Subtle or even hidden correlations between different imaging modalities may well be unraveled through high-throughput tests and deep-learning-assisted image recognition/mining. Significantly higher coherent flux facilitated with rapid advances in data analysis and computation will make X-ray microscopy methods such as ptychography far more accessible and efficient in the near future, which could introduce high-spatiotemporal-resolution 4D (*x*, *y*, *z*, *t*) characterizations of HP material microstructures in realistic operation environments or conditions.[61] It is anticipated that the optoelectronic process in its intrinsic time scale is more fundamental to the formation of the optoelectronic property. Transient-state studies of the optoelectronic process, with the excitation of a single short X-ray pulse, at the time scale of subnanosecond to tens of nanoseconds, can provide insights into the optoelectronic behavior of HPs. Combining the transient process technique with X-ray microscopy, one can further study the intrinsic optoelectronic process as functions of local chemistry and structure (relevant development has taken place, for example, at the sector 26-ID-C of the APS).

The long-term material and device operation stability poses a very demanding challenge to the development and commercialization of HP materials for all proclaimed energy and optoelectronic technology applications. The aging and degrading mechanisms of HP material and devices require a thorough and deep understanding of complex fading processes across the entire hierarchy of length scales and time scales, which highly demands the characterization beyond simple equilibrium phenomena and beyond models based on idealized materials and systems. In this regard, coherent X-ray photon correlation spectroscopy (XPCS) based on a statistical analysis of the evolution of the speckle patterns as a function time or an externally varied quantity, such as light exposure, electric field, or heating, will provide indispensable insights into the dynamic evolution of material nucleation, structural transformations, and domain fluctuations during complex growth and fading processes under realistic conditions.[62] In practical terms, the ultimate accessible time resolution of XPCS measurements is proportional to the square of the coherent flux and also the square of the brightness. Consequently, this dynamic probing technique will be the biggest beneficiary of storage ring MBA lattice upgrade as it will be for post-APS-U XPCS beamlines, whereby nanosecond-resolution studies of meso-/nanoscale fluctuations for correlations detected within the duration of X-ray exposures would be well expected.

The new-generation highly brilliant synchrotron source will make it practical and routine to carry out multimodal experiments spanning vast ranges of characteristic times and spatial scales. Such developments would be matched well by simultaneous advances in data analysis, theory, and computation that will deliver new integration and cooperation of simulations and experiments. For instance, the structural, chemical, and electronic configurative information of various HP thin films and devices using post-APS-U X-ray beams will be acquired and rendered in grain-by-grain or domain-by-domain manner rather than statistical ensemble or average. New methods for extracting deep insights from massive volumes of data and new parameters that can then be incorporated into thermodynamic and mechanistic models of materials will be developed for the upgraded X-ray facilities to probe sophisticated systems and complex processes previously impractical to investigate with precision. Advances in computation are well positioned to afford rapid multidimensional data analysis to 2D/3D X-ray microscopy measurements to enable simulations to be performed in the course of experimental observations, and to endow new

tools combining near-real-time modeling, data acquisition, and advanced analytic methods.[63] Tremendous flexibilities in chemical compositions and structural building blocks have shaped HP systems into an unprecedented materials family with an almost unlimited number of derivative and extended members. The HP material explorations including crystal structure determination, elemental profiling, and functionality screening can be facilitated by high-throughput multimodal X-ray characterizations intelligently guided by data-driven strategies for optimizing structural and chemical precursors and predicting emerging properties and functionalities.[64] Last but not least, benefits of many ongoing developments of *in situ/operando* experiments as illustrated and foreseen in this perspective to emulate the real-world industrial process of HP materials into commercial metric and scalable devices will fill the gap and encourage the leap forward from fundamental studies to truly practical guidelines. Although without a doubt still in the R&D incubation stage for HP materials and devices, the compelling capability of these synchrotron-based X-ray techniques should entice a broad range of industrial researchers and leverage maturation endeavors.

In closing, we envision that synchrotron characterization of HPs will rise rapidly as an exciting interdisciplinary research area that will be full of surprising science discoveries.

ACKNOWLEDGMENTS

Y.Z. acknowledges funding support from the National Science Foundation (nos. OIA-1538893 and OIA-1929019), Office of Naval Research (N00014-17-1-2232), and the generous support from Prof. Nitin Padture at Brown University. H.Z., J.D., W.C., and Z.C. acknowledge the support of the Advanced Photon Source and the Center for Nanoscale Materials, a US Department of Energy (DOE) Office of Science User Facility operated for the DOE Office of Science by Argonne National Laboratory under contract no. DE-AC02-06CH11357. The authors also acknowledge Dr. J. Gong and a group of other APS scientists for valuable discussions.

AUTHOR CONTRIBUTIONS

Y.Z. conceived the idea. Y.Z. and H.Z. co-drafted the article. All authors contributed to the writing of this article.

REFERENCES

1. Kojima, A., Teshima, K., Shirai, Y., and Miyasaka, T. (2009). Organometal halide perovskites as visible-light sensitizers for photovoltaic cells. J. Am. Chem. Soc. *131*, 6050–6051.

2. Snaith, H.J. (2018). Present status and future prospects of perovskite photovoltaics. Nat. Mater. *17*, 372–376.

3. Dunlap-Shohl, W.A., Zhou, Y., Padture, N.P., and Mitzi, D.B. (2019). Synthetic approaches for halide perovskite thin films. Chem. Rev. *119*, 3193–3295.

4. Saparov, B., and Mitzi, D.B. (2016). Organic-inorganic perovskites: structural versatility for functional materials design. Chem. Rev. *116*, 4558–4596.

5. Zhang, W., Eperson, G.E., and Snaith, H.J. (2016). Metal halide perovskites for energy applications. Nat. Energy *1*, 16048.

6. NREL best research-cell efficiency chart. https://www.nrel.gov/pv/cell-efficiency.html.

7. Raino, G., Becker, M.A., Bodnarchuk, M.I., Mahrt, R.F., Kovalenko, M.V., and Stoferle, T. (2018). Superfluorescence from lead halide perovskite quantum dot superlattices. Nature *563*, 671–675.

8. Utzat, H., Sun, W.W., Kaplan, A.E.K., Krieg, F., Ginterseder, M., Spokoyny, B., Klein, N.D., Shulenberger, K.E., Perkinson, C.F., Kovalenko, M.V., and Bawendi, M.G. (2019). Coherent single-photon emission from colloidal lead halide perovskite quantum dots. Science *363*, 1068–1072.

9. Mao, L., Stoumpos, C.C., and Kanatzidis, M.G. (2019). Two-dimensional hybrid halide perovskites: principles and promises. J. Am. Chem. Soc. *141*, 1171–1190.

10. Ju, M.-G., Chen, M., Zhou, Y., Dai, J., Ma, L., Padture, N.P., and Zeng, X.C. (2018). Toward eco-friendly and stable perovskite materials for photovoltaics. Joule *2*, 1231–1241.

11. Lin, H.R., Zhou, C.K., Tian, Y., Siegrist, T., and Ma, B. (2018). Low-dimensional organometal halide perovskites. ACS Energy Lett. *3*, 54–62.

12. Zhou, Y., Game, O.S., Pang, S., and Padture, N.P. (2015). Microstructures of organometal trihalide perovskites for solar cells: their evolution from solutions and characterization. J. Phys. Chem. Lett. *6*, 4827–4839.

13. Zhou, Y., Zhou, Z., Chen, M., Zong, Y., Huang, J., Pang, S.P., and Padture, N.P. (2016). Doping and alloying for improved perovskite solar cells. J. Mater. Chem. A *4*, 17623–17635.

14. Stuckelberger, M., West, B., Nietzold, T., Lai, B., Maser, J.M., Rose, V., and Bertoni, M.I. (2017). Engineering solar cells based on correlative X-ray microscopy. J. Mater. Res. *32*, 1825–1854.

15. Robinson, I., and Harder, R. (2018). Coherent X-ray diffraction imaging of strain at the nanoscale. Nat. Mater. *8*, 291–298.

16. Pfeiffer, F. (2018). X-ray ptychography. Nat. Photon. *12*, 9–17.

17. Xiao, C., Li, Z., Guthrey, H., Moseley, J., Yang, Y., Wozny, S., Moutinho, H., To, B., Berry, J.J., Gorman, B., et al. (2015). Mechanisms of electron-beam-induced damage in perovskite thin films revealed by cathodoluminescence spectroscopy. J. Phys. Chem. C *119*, 26904–26911.

18. Deng, J., Preissner, C., Klug, J.A., Mashrafi, S., Roehrig, C., Jiang, Y., Yao, Y., Wojcik, M., Wyman, M.D., Vine, D., et al. (2019). The velociprobe: an ultrafast hard X-ray nanoprobe for high-resolution ptychographic imaging. Rev. Sci. Instrum. *90*, 083701.

19. Nagaoka, Y., Hills-Kimball, K., Tan, R., Li, R., Wang, Z., and Chen, O. (2017). Nanocube superlattices of cesium lead bromide perovskites and pressure-induced phase transformations at atomic and mesoscale levels. Adv. Mater. *29*, 1606666.

20. Soe, C.M.M., Nagabhushana, G.P., Shivaramaiah, R., Tsai, H.H., Nie, W., Blancon, J.C., Melkonyan, F., Cao, D., Traore, B., Pedesseau, L., et al. (2019). Structural and thermodynamic limits of layer thickness in 2D halide perovskites. Proc. Natl. Acad. Sci. U S A *116*, 58–66.

21. Leguy, A.M.A., Frost, J.M., McMahon, A.P., Sakai, V.G., Kockelmann, W., Law, C., Li, X.E., Foglia, F., Walsh, A., O'Regan, B.C., et al. (2015). The dynamics of methylammonium ions in hybrid organic-inorganic perovskite solar cells. Nat. Commun. *6*, 7124.

22. Bertolotti, F., Protesescu, L., Kovalenko, M.V., Yakunin, S., Cervellino, A., Billinge, S.J.L., Terban, M.W., Pedersen, J.S., Masciocchi, N., and Guagliardi, A. (2017). Coherent nanotwins and dynamic disorder in cesium lead halide perovskite nanocrystals. ACS Nano *11*, 3819–3831.

23. Adhyaksa, G.W.P., Brittman, S., Abolins, H., Lof, A., Li, X., Keelor, J.D., Luo, Y., Duevski, T., Heeren, R.M.A., Ellis, S.R., et al. (2018). Understanding detrimental and beneficial grain boundary effects in halide perovskites. Adv. Mater. *30*, 1804792.

24. Correa-Baena, J.-P., Luo, Y., Brenner, T.M., Snaider, J., Sun, S., Li, X., Jensen, M.A., Hartono, N.T.P., Nienhaus, L., Wieghold, S., et al. (2019). Homogenized halides and alkali cation segregation in alloyed organic-inorganic perovskites. Science *363*, 627–631.

25. Whitfield, P.S., Herron, N., Guise, W.E., Page, K., Cheng, Y., Milas, I., and Crawford, M.K. (2016). Structures, phase transitions and tricritical behavior of the hybrid perovskite methyl ammonium lead iodide. Sci. Rep. *6*, 35685.

26. Jiang, S., Luan, Y., Jang, J., Baikie, T., Huang, X., Li, R., Saouma, F.O., Wang, Z., White, T.J., and Fang, J. (2018). Phase transitions of formamidinium lead iodide perovskite under pressure. J. Am. Chem. Soc. *140*, 13952–13957.

27. Schelhas, L.T., Christians, J.A., Berry, J.J., Toney, M.F., Tassone, C.J., Luther, J.M., and Stone, K.H. (2016). Monitoring a silent phase transition in $CH_3NH_3PbI_3$ solar cells via operando X-ray diffraction. ACS Energy Lett. *1*, 1007–1012.

28. Jones, T.W., Osherov, A., Alsari, M., Sponseller, M., Duck, B.C., Jung, Y.K., Settens, C., Niroui, F., Brenes, R., Stan, C.V., et al. (2019). Lattice strain causes non-radiative losses in halide perovskites. Energy Environ. Sci. *12*, 596–606.

29. Li, X., Luo, Y., Holt, M.V., Cai, Z., and Fenning, D.P. (2019). Residual nanoscale strain in cesium lead bromide perovskite reduces stability and shifts local luminescence. Chem. Mater. *31*, 2778–2785.

30. Hu, Q., Zhao, L., Wu, J., Gao, K., Luo, D.Y., Jiang, Y., Zhang, Z., Zhu, C., Schaible, E., Hexemer, A., et al. (2017). In situ dynamic observations of perovskite crystallisation and microstructure evolution intermediated from $[PbI_6]^{4-}$ cage nanoparticles. Nat. Commun. *8*, 15688.

31. Bruening, K., and Tassone, C.J. (2018). Antisolvent processing of lead halide perovskite thin films studied by in situ X-ray diffraction. J. Mater. Chem. A *6*, 18865–18870.

32. Chen, A.Z., Shiu, M., Ma, J., Alpert, M.R., Zhang, D., Foley, B.J., Smilgies, D.M., Lee, S.H., and Choi, J.J. (2018). Origin of vertical orientation in two-dimensional metal halide perovskites and its effect on photovoltaic performance. Nat. Commun. *9*, 1336.

33. Zhao, J., Cai, B., Luo, Z., Dong, Y.Q., Zhang, Y., Xu, H., Hong, B., Yang, Y.J., Li, L.B., Zhang, W., and Gao, C. (2016). Investigation of the hydrolysis of perovskite organometallic halide $CH_3NH_3PbI_3$ in humidity environment. Sci. Rep. *6*, 21976.

34. Stuckelberger, M., Nietzold, T., Hall, G.N., West, B., Werner, J., Niesen, B., Ballif, C., Rose, V., Fenning, D.P., and Bertoni, M.I. (2017). Charge collection in hybrid perovskite solar cells: relation to the nanoscale elemental distribution. IEEE J. Photovoltaics *7*, 590–597.

35. Luo, Y., Aharon, S., Stuckelberger, M., Magana, E., Lai, B., Bertoni, M.I., Etgar, L., and Fenning, D.P. (2018). The relationship between chemical flexibility and nanoscale charge collection in hybrid halide perovskites. Adv. Funct. Mater. *28*, 1706995.

36. Steele, J.A., Jin, H., Dovgaliuk, I., Berger, R.F., Braeckevelt, T., Yuan, H., Martin, C., Solano, E., Lejaeghere, K., Rogge, S.M.J., et al. (2019). Thermal unequilibrium of strained black $CsPbI_3$ thin films. Science *365*, 679–684.

37. Saliba, M., Matsui, T., Seo, J.Y., Domanski, K., Correa-Baena, J.P., Nazeeruddin, M.K., Zakeeruddin, S.M., Tress, W., Abate, A., Hagfeldt, A., and Gratzel, M. (2016). Cesium-containing triple cation perovskite solar cells: improved stability, reproducibility and high efficiency. Energy Environ. Sci. *9*, 1989–1997.

38. Chen, Q., Chen, L., Ye, F., Zhao, T., Tang, F., Rajagopal, A., Jiang, Z., Jiang, S.L., Jen, A.K.-Y., Xie, Y., et al. (2017). Ag-incorporated organic-inorganic perovskite films and planar heterojunction solar cells. Nano Lett. *17*, 3231–3237.

39. Philippe, B., Saliba, M., Correa-Baena, J.P., Cappel, U.B., Turren-Cruz, S.H., Gratzel, M., Hagfeldt, A., and Rensmo, H. (2017). Chemical distribution of multiple cation (Rb^+, Cs^+, MA^+, and FA^+) perovskite materials by photoelectron spectroscopy. Chem. Mater. *29*, 3589–3596.

40. Abdi-Jalebi, M., Pazoki, M., Philippe, B., Dar, M.I., Alsari, M., Sadhanala, A., Diyitini, G., Imani, R., Lilliu, S., Kullgren, J., et al. (2018). Dedoping of lead halide perovskites incorporating monovalent cations. ACS Nano *12*, 7301–7311.

41. Zhou, Y., Sternlicht, H., and Padture, N.P. (2019). Transmission electron microscopy of halide perovskite materials and devices. Joule *3*, 641–661.

42. Li, W., Yadavalli, S.K., Lizarazo-Ferro, D., Chen, M., Zhou, Y., Padture, N.P., and Zia, R. (2018). Subgrain special boundaries in halide perovskite thin films restrict carrier diffusion. ACS Energy Lett. *3*, 2669–2670.

43. Rothmann, M.U., Li, W., Zhu, Y., Bach, U., Spiccia, L., Etheridge, J., and Cheng, Y.-B. (2017). Direct observation of intrinsic twin domains in tetragonal $CH_3NH_3PbI_3$. Nat. Commun. *8*, 14547.

44. Zhao, J., Deng, Y., Wei, H., Zheng, X., Yu, Z., Shao, Y., Shield, J.E., and Huang, J. (2017). Strained hybrid perovskite thin films and their impact on the intrinsic stability of perovskite solar cells. Sci. Adv. *3*, eaao5616.

45. Pedersen, E.B.L., Angmo, D., Dam, H.F., Thydén, K.T.S., Andersen, T.R., Skjønsfjell, E.T.B., Krebs, F.C., Holler, M., Diaz, A., Guizar-Sicairos, M., et al. (2015). Improving organic tandem solar cells based on water-processed nanoparticles by quantitative 3D nanoimaging. Nanoscale *7*, 13765–13774.

46. Deng, J., Lo, Y.H., Gallagher-Jones, M., Chen, S., Pryor, A., Jin, Q., Hong, Y.P., Nashed, Y.S.G., Vogt, S., Miao, J., and Jacobsen, C. (2018). Correlative 3D X-ray fluorescence and ptychographic tomography of frozen-hydrated green algae. Sci. Adv. *4*, eaau4548.

47. Shapiro, D.A., Yu, Y.-S., Tyliszczak, T., Cabana, J., Celestre, R., Chao, W., Kaznatcheev, K., Kilcoyne, A.L.D., Maia, F., Marchesini, S., et al. (2014). Chemical composition mapping with nanometre resolution by soft X-ray microscopy. Nat. Photon. *8*, 765–769.

48. Hirose, M., Ishiguro, N., Shimomura, K., Nguyen, D.-N., Matsui, H., Dam, H.C., Tada, M., and Takahashi, Y. (2019). Oxygen-diffusion-driven oxidation behavior and tracking areas visualized by X-ray spectro-ptychography with unsupervised learning. Commun. Chem. *2*, 50.

49. Yau, A., Cha, W., Kanan, M.W., Stephenson, G.B., and Ulvestad, A. (2017). Bragg coherent diffractive imaging of single-grain defect dynamics in polycrystalline films. Science *356*, 739–742.

50. Alsari, M., Bikondoa, O., Bishop, J., Abdi-Jalebi, M., Ozer, L.Y., Hampton, M., Thompson, P., Horantner, M.T., Mahesh, S., Greenland, C., et al. (2018). In situ simultaneous photovoltaic and structural evolution of perovskite solar cells during film formation. Energy Environ. Sci. *11*, 383–393.

51. Stone, K.H., Gold-Parker, A., Pool, V.L., Unger, E.L., Bowring, A.R., McGehee, M.D., Toney, M.F., and Tassone, C.J. (2018). Transformation from crystalline precursor to perovskite in $PbCl_2$-derived $MAPbI_3$. Nat. Commun. *9*, 3458.

52. Miyadera, T., Shibata, Y., Koganezawa, T., Murakami, T.N., Sugita, T., Tanigaki, N., and Chikamatsu, M. (2015). Crystallization dynamics of organolead halide perovskite by real-time X-ray diffraction. Nano Lett. *15*, 5630–5634.

53. Schmidt-Hansberg, B., Sanyal, M., Klein, M.F.G., Pfaff, M., Schnabel, N., Jaiser, S., Vorobiev, A., Muller, E., Colsmann, A., Scharfer, P., et al. (2011). Moving through the phase diagram: morphology formation in solution cast polymer-fullerene blend films for organic solar cells. ACS Nano *5*, 8579–8590.

54. Schelhas, L.T., Li, Z., Christians, J.A., Goyal, A., Kairys, P., Harvey, S.P., Kim, D.H., Stone, K.H., Luther, J.M., Zhu, K., et al. (2019). Insights into operational stability and processing of halide perovskite active layers. Energy Environ. Sci. *12*, 1341–1348.

55. Yang, J., Siempelkamp, B.D., Liu, D., and Kelly, T.L. (2015). Investigation of $CH_3NH_3PbI_3$ degradation rates and mechanisms in controlled humidity environments using in situ techniques. ACS Nano *9*, 1955–1963.

56. Wang, Y., Lu, X., Yang, W., Wen, T., Yang, L., Ren, X., Wang, L., Lin, Z., and Zhao, Y. (2015). Pressure-induced phase transformation, reversible amorphization, and anomalous visible light response in organolead bromide perovskite. J. Am. Chem. Soc. *137*, 11144–11149.

57. Liu, G., Gong, J., Kong, L.P., Schaller, R.D., Hu, Q., Liu, Z., Yan, S., Yang, W., Stoumpos, C.C., Kanatzidis, M.G., et al. (2018). Isothermal pressure-derived metastable states in 2D hybrid perovskites showing enduring bandgap narrowing. Proc. Natl. Acad. Sci. U S A *115*, 8076–8081.

58. Pacchioni, G. (2019). An upgrade to a bright future. Nat. Rev. Phys. *1*, 100.

59. Dosch, H. (2019). European accelerator-based photon sources join forces. Nat. Rev. Mater. *4*, 459.

60. Eriksson, M., van der Veen, J.F., and Quitmann, C. (2014). Diffraction-limited storage rings—a window to the science of tomorrow. J. Synchrotron Radiat. *21*, 837–842.

61. Hitchcock, A.P., and Toney, M.F. (2014). Spectromicroscopy and coherent diffraction imaging: focus on energy materials applications. J. Synchrotron Radiat. *21*, 1019–1030.

62. Shpyrko, O.G. (2014). X-ray photon correlation spectroscopy. J. Synchrotron Radiat. *21*, 1057–1064.

63. Wang, C., Steiner, U., and Sepe, A. (2018). Synchrotron big data science. Small *14*, e1802291.

64. Ren, F., Ward, L., Williams, T., Laws, K.J., Wolverton, C., Hattrick-Simpers, J., and Mehta, A. (2018). Accelerated discovery of metallic glasses through iteration of machine learning and high-throughput experiments. Sci. Adv. *4*, eaaq1566.